Dynamics of the Coulomb explosion of large clusters in a strong laser field

Isidore Last and Joshua Jortner
School of Chemistry, Tel-Aviv University, Ramat Aviv, Tel Aviv 69978, Israel
(Received 30 November 1999; published 8 June 2000)

The multielectron ionization and Coulomb explosion of Xe_{55}, Xe_{249}, Xe_{531}, and Xe_{1061} clusters in a strong laser field is studied using classical dynamics simulations, which describe the motion of unbound electrons and ions. The generation of the unbound electrons is described as the removal of bound electrons from their host atoms (ions) by the electrostatic barrier suppression or collisional ionization. According to the results of simulations performed for the laser power 10^{16} W/cm^2 and frequency 0.386 fs^{-1}, almost all unbound electrons are removed from the clusters. In large Xe_{531} and Xe_{1061} clusters, electrons are removed mainly when the size of the clusters is enlarged due to Coulomb explosion. The quasiresonance energy enhancement is shown to be mainly responsible for the removal of electrons from the clusters. The energy enhancement process is hampered by electron-electron and electron-ion collisions.

PACS number(s): 36.40.Gk

I. INTRODUCTION

Clusters are often considered as bridge systems between isolated molecules and the condensed phase. Such a point of view is supported by the multitude of observations that most of the properties of clusters, apart from specific cluster size effects, are changing more or less monotonously with their size, being close to those of isolated molecules and condensed phase systems in the limiting cases of small and large clusters, respectively [1–3]. An exception to such a regularity in the cluster behavior is exhibited by the phenomenon of multielectron dissociative ionization (MEDI) [4–13].

The MEDI phenomenon was first detected in molecules [4–6]. When a molecule is subjected to a strong laser field ($S > 10^{13}$ W/cm^2) all atoms of this molecule become ionized, leading to Coulomb explosion and the production of atomic ions. The kinetic energy of the product atomic ions of the MEDI process is expected to increase with the size of a system [14], being of the order of several or tens of eV in diatomic molecules [4–6] and hundreds of eV in small, $n \leqslant 13$ clusters [7,8]. In large clusters composed of $n \approx 10^3 - 10^5$ atoms, the kinetic energy of the product ions becomes extremely high, mostly of the order of tens or hundreds of keV, reaching in clusters composed of $n \sim 10^5$ nuclear energy scale values of about 1 MeV [9–13]. In large clusters, the product ions are mostly highly ionized, up to a charge per ion of $q = +40$ in the case of xenon clusters [9–13]. The Coulomb explosion of large clusters may be also accompanied by x-ray generation [15]. The increase of the MEDI efficiency with the cluster size cannot be extrapolated smoothly to very large ($n \gg 10^5$, probably) clusters since in the limit case of the condensed phase the MEDI process does not take place at all. The highly efficient MEDI of large ($n \sim 10^3 - 10^5$) clusters is a unique phenomenon, which differs in a significant way from the MEDI of molecules and small clusters, and it has no analogy in solids and liquids.

The MEDI of a diatomic molecule may be described by the charge resonance enhancement ionization (CREI) mechanism [16–18]. This mechanism connects the electron energy enhancement with an inner potential barrier, which separates the potential wells inside the molecule. The inner barrier increases with the interatomic distance R preventing at some distance R_b the classical electron motion between the two atoms (ions) so that at $R > R_b$ the electron can jump between the two atoms (ions) due to tunneling only. In a strongly charged molecule, the tunneling may provide conditions for the quasiresonance enhancement of the electron energy and consequently for the electron removal from the molecule [19,20]. As has recently been shown by us, more effective ionization is provided by the dynamic mechanism of the quasiresonance energy enhancement [18]. According to this mechanism, which is of classical origin, the electron energy may increase simultaneously with the rise of the inner barrier. This mechanism was also shown to take place in small clusters [18].

In a large multicharged cluster, the inner potential barriers cannot play any important role in the process of energy enhancement because the energy of the unbound electrons is high, being well above the inner barriers [21]. We will show that in such a cluster the quasiresonance enhancement of the unbound electron energy is realized while these electrons oscillate inside the cluster or in the space around it. The mechanism of the electron removal from a cluster (outer ionization) was studied recently through a classical dynamics simulation of electron motion in the approximation of fixed cluster geometry and a fixed number of unbound electrons [22]. In the present work we perform the full-scale classical dynamics simulation, considering both the light (electrons) and the heavy (ions) particle motion and taking into account the generation of unbound electrons by inner ionization processes. A similar dynamics simulation was performed recently by Ditmire but only for small, up to $n = 55$, Ar_n clusters [23].

It is also of considerable interest to study theoretically the MEDI process in large clusters, which exhibit features different from those of small clusters [9]. In the present work we will treat relatively large Xe_n clusters, up to $n = 1061$. We chose Xe clusters because in a strong laser field Xe atoms can be deprived not only of their outer shell electrons, like in the case of Ar atoms, but also of their inner *d*-shell electrons,

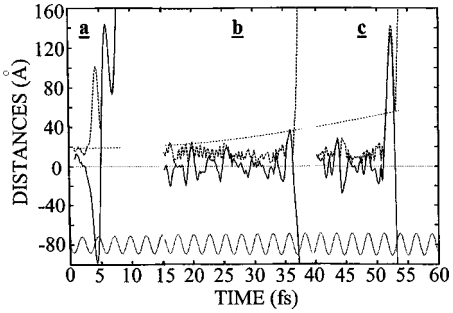

FIG. 1. Three electron trajectories in the Xe_{531} cluster. Trajectories (b) and (c) are presented not from the beginning but only for the time intervals that precede the ionization event. Irradiation parameters: maximal power, $S_{max}=10^{16}\,W/cm^2$; frequency, $\nu=0.386\,fs^{-1}$: —, electron motion along the laser field polarization; --, electron distance from the cluster center; ---, cluster radius; ⋯, the laser field (in arbitrary units).

providing the opportunity to study the formation of strongly charged, $q>8$, ions.

II. METHODOLOGY OF THE DYNAMICS SIMULATIONS

The process of cluster ionization and Coulomb explosion involves three different kinds of particles: the electrons bound to host ions, the unbound electrons, and the heavy particles (ions). The most complicated problem is presented by the bound electrons because their motion is of quantum origin. In the present dynamic simulations of cluster ionization we shall follow the work of Ref. [23] with the bound electrons not being explicitly treated, and the inner ionization being described as the generation of unbound electrons by ions (atoms) when the conditions for inner ionization are fulfilled.

The unbound electrons can be treated classically when their de Broglie wavelength λ is considerably smaller than the internuclear spacing d. According to Fig. 1, which presents three electron trajectories, electrons oscillate inside the cluster. The kinetic energy of these oscillations (Fig. 2) exceeds mostly 33 eV, with the energy corresponding to $\lambda=d/2=2.2$ Å. It follows that quantum effects of the electron motion are not of much importance, so that the classical approach can be accepted. The classical approach is obviously applicable for the simulation of heavy particles. The interaction of electrons with the very strong laser field is also of a classical character due to the large number of photons involved [24]. It follows that the simulation of the MEDI process of large clusters in the framework of classical mechanics is quite substantiated.

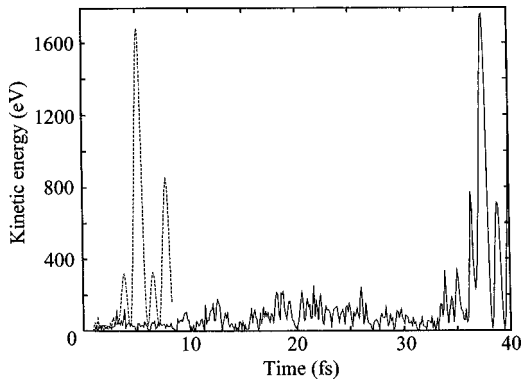

FIG. 2. Kinetic energy of the trajectories presented in Fig. 1 as (a) and (b).

In our classical dynamics simulation, we have to take into account three kinds of interactions, namely, electron-electron, electron-ion, and ion-ion interactions. The Coulomb potential of the electron-electron interaction is modified by a smoothing term in order to avoid a steep increase in forces at very small distances and the violation of energy conservation [22]:

$$U_{e-e}=\frac{B}{\sqrt{r^2+r_0^2}}, \tag{1}$$

where $B=14.385$ eV Å and the smoothing parameter is taken as $r_0=0.2$ Å. This value was chosen as the minimal smoothing parameter, which does not violate the energy conservation. We note in passing that in Ref. [22] there was a misprint in the r_0 value, but the calculations were performed with the correct parameter given above.

The potential of the electron-ion interaction is expressed as the sum of the Coulomb attractive potential and a short-range repulsive term [22]. The short-range term simulates the repulsive component of the electron-ion interaction and also prevents the penetration of electrons into the inner core region of very high Coulomb forces, which may result in the violation of energy conservation. It is generally accepted to present the repulsive term as an exponential function [25]. In such a presentation, however, the penetration of energetic electrons into the inner core region of ions is not prevented. To this end the power function $r^{-\eta}$ serves much better [22]. The potential of the electron interaction with a neutral atom is provided in Ref. [25]. This potential is well fitted by the power function C_q/r^6, where q is the ion charge, with $C_{q=0}=70$ eV Å^6 [22]. We use the C_q/r^6 function to describe the repulsive potential for an arbitrary q, presenting the electron-ion interaction potential as

$$U_{e-q}=-\frac{Bq}{r}+\frac{C_q}{r^6}. \tag{2}$$

Unfortunately, the C_q parameters for $q>0$ cannot be determined directly since there are no data for the electron-ion interactions. It is reasonable to suggest only that the C_q parameter decreases with q. However, the need to prevent the violation of energy conservation compels us to limit the C_q coefficient from below. It was found that this limit is $C_q\approx 0.5$ eV Å^6. In order to produce the C_q coefficient for any ionic charge q, we express C_q by a simple and to some extent arbitrary relation, which provides a correct number for $q=0$ (70 eV Å^6) and meets the condition $C_q>0.5$ eV Å^6:

$$C_q=0.5+\frac{840}{I_q}, \tag{3}$$

where I_q is the ionization potential (in eV) of the q-fold charged ion.

The ion-ion interactions are described by a Coulomb potential. All other interactions between ions or neutral atoms are ignored in our simulation. Such an approach is feasible since in a strong laser field atoms quickly lose one or more electrons so that the Coulomb potential becomes the dominant interaction [22], in contrast to the case of the weakly charged clusters [26].

The laser field force acting on an electron is

$$eF_l = eF_0 \cos(2\pi\nu t + \varphi_0), \tag{4}$$

where F_0, ν, and φ_0 are the laser field amplitude, frequency, and initial phase, respectively. We also take into account the forces generated by the magnetic component of the laser field. We found the magnetic-field effect on the ionization process to be of minor importance.

Initially, prior to the switching on of the laser field, the cluster is composed of neutral atoms. After the laser field is switched on, the process of inner ionization starts, resulting in the bound electron removal from their host atoms and the transformation of neutral atoms into charged ions. The unbound electrons generated by the inner ionization may be removed from the cluster to infinity, presenting the process of outer ionization. In order to describe the outer ionization we simulate the motion of the unbound electrons. However, in order to know the number of unbound electrons, one also needs to simulate the inner ionization process. The inner ionization can be realized by two mechanisms: the suppression of the electrostatic barriers of the host ions (suppression mechanism) and the electron collisional ionization.

Let us consider first the suppression mechanism. The condition for the inner ionization is the suppression of a potential barrier, which keeps a bound electron inside its host atom (ion) subjected to an external electrostatic field. Initially, in the neutral cluster, only the outer laser field can be responsible for the inner ionization of atoms. However, after the neutral atoms are ionized by the outer field and some of the unbound electrons are removed from the cluster, the cluster becomes charged, providing an electrostatic field that may enhance the inner ionization of the cluster ions (the so-called ignition mechanism [27]). Considering the electron-host ion interaction in the Coulomb approximation, one obtains the following condition for the electrostatic barrier suppression:

$$|eF| > I_q^2/4B(q+1), \tag{5}$$

where F is the field generated by the laser and the charged particles of the cluster.

The probability of the collisional ionization of a single atom (ion) can be estimated by Lotz's expression for the ionization cross section [28]. When applied to the ionization of the i-fold ionized ion with $i=q$, this expression is

$$\sigma_i = a\sum_{j=1}^{J}\left(\frac{1}{KI_j}\right)\ln\left(\frac{K}{I_j}\right), \tag{6}$$

where $a = 450\,(\mathrm{eV})^2\,\text{Å}^2$, K is the kinetic energy of the impact electron, I_j is the ionization potential of the j-fold ionized ion ($j \geqslant i$), and $I_J < K < I_{J+1}$. We suggest that one take into account only the first term in Eq. (6), whose contribution to σ_i dominates. In this approximation, we take $i=q$ and the ionization impact parameter is

$$b_q = \frac{1}{\pi}\sqrt{\frac{a}{KI_q}\ln\left(\frac{K}{I_q}\right)}. \tag{7}$$

The ionization takes place when the impact parameter b of the incident electron is smaller than the ionization impact parameter:

$$b < b_q. \tag{8}$$

The impact parameters b and b_q are obviously related to infinite initial electron-ion distance. However, when performing dynamic simulations in a dense system, one can determine the incident electron parameters on a finite distance from an ion only. Consequently, the problem that arises involves finding the connection between the local (at a finite distance) parameters and those at infinity for the incident electron. We suggest that the local parameters at an electron-ion distance r_l, which is significantly smaller than the interatomic distance, be determined so that the collision can be treated in the same way as for an isolated electron-ion pair. The distance r_l is assumed, however, to be significantly large to ignore the short-range repulsive term of Eq. (2). This condition can be easily fulfilled for $q>1$ since in this case the repulsive term, according to Eqs. (2) and (3), contributes significantly only at distances much smaller than the interatomic distance. Suggesting that r_l is the distance where the repulsive term is ten times smaller than the Coulomb potential, one obtains for $q=2$ and 3 $r_l = 1.5$ and 1.0 Å, respectively, whereas the interatomic distance is larger than 4.3 Å. The situation is worse for $q=0$ and 1. Using the same criterion for $q=1$ we obtain $r_l = 1.9\,\text{Å}$, which is somewhat, but not much, smaller than the interatomic distance. We also use the same r_l distance for a neutral atom, $q=0$, in spite of the fact that at this distance the repulsive interaction is not small, being about 1.5 eV. Fortunately, as will be shown in Sec. III, the neutral atoms are not of much importance since all atoms are ionized in the very beginning of the ionization process. Ignoring the repulsive term at $r > r_l$, we are left with a pure Coulomb potential that makes the connection between the kinetic energy at infinity (K) and at r_l (K_l) quite trivial:

$$K = K_l - \frac{Bq}{r_l}. \tag{9}$$

It is much more difficult to find the connection between the impact parameter at infinity b and the local impact parameter b_l determined at the finite distance r_l:

$$b_l = \vec{v}_l \cdot \vec{r}_l / v_l, \tag{10}$$

where $\vec{r}_l$ is the radius vector directed from the incident electron toward the attacked ion and $\vec{v}_l$ is the electron velocity at $\vec{r}_l$. In order to find this connection, we performed the simulation of the incident electron motion in the Coulomb field of

the attacked ion. The results of the simulation allowed us to fit the impact parameter b's dependence on b_l by an analytical expression

$$b=\frac{1+\xi}{\xi}\left[1+\frac{\eta}{1+\eta}\right]b_l, \tag{11a}$$

where

$$\xi=0.159 r_l K/q, \tag{11b}$$

$$\eta=0.4\left(\frac{b_l}{r_l}\right)^2. \tag{11c}$$

Equation (11a) is valid for condition $\eta \ll 1$, which can be readily fulfilled.

When treating the collisional ionization in a charged cluster, we also have to take into account that the IP I_q of Eq. (7) differs from that of an isolated ion. In a charged cluster, the inner ionization does not mean electron removal to infinity, but to some interionic space where the electron becomes unbound (delocalized). It follows that instead of using the IP I_q of an isolated ion, we have to use a smaller value of

$$I_q'=I_q-\frac{Bq}{r'}, \tag{12}$$

where r' is of the order of half of the interionic distance.

The outer ionization event is recorded when the distance R_O between an electron and the cluster center is large enough to ignore the interaction of this electron with other electrons. This condition was found to be met when the distance R_O was at least 15 times larger than the cluster effective radius $R_{\rm cl}$:

$$R_O > 15 R_{\rm cl}. \tag{13}$$

The effective radius $R_{\rm cl}$ is determined as the mean-square root of the atom distribution

$$R_{\rm cl}=\sqrt{\frac{1}{n}\sum_{i=1}^{n} R_i^2}, \tag{13'}$$

where R_i are the atomic distances from the center of mass. After the act of the outer ionization is recorded in accordance with condition (13) the electron is discarded from the simulation procedure. Consequently, the number of electrons in the system $N_e(t)$ is equal to the difference between the number of electrons $N_{\rm ii}(t)$ generated by the inner ionization processes and the number of electrons $N_{\rm oi}(t)$ removed by the outer ionization process:

$$N_e(t)=N_{\rm ii}(t)-N_{\rm oi}(t). \tag{14}$$

In our dynamic simulations, the classical equations of the motion of light particles (unbound electrons) are solved using the time steps of 5×10^{-4} fs. These ultrashort time steps are necessary for the simulation of the dynamics of the light particles, and were chosen to ensure the energy conservation. In the case of heavy particles (ions), the time steps are much larger, mostly of the order of 0.1 fs. These time steps have been shown to provide stable simulation results.

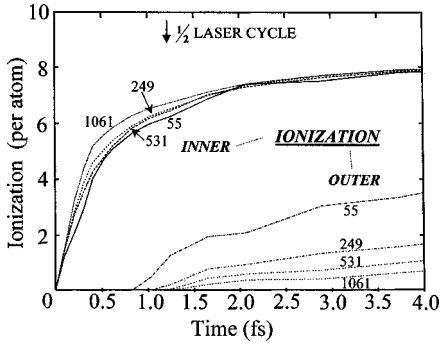

FIG. 3. Ionization dynamics in the first 4 fs of irradiation. The upper lines denote inner ionization, the lower ones outer ionization. The numbers indicate the cluster size. Irradiation parameters as in Fig. 1.

III. SIMULATION RESULTS

Dynamic simulations have been performed for Xe_{55}, Xe_{249}, Xe_{531}, and Xe_{1061} clusters (initial radii $R_0=8.7$, 15.0, 18.9, and 24.9 Å, respectively; interatomic distance of 4.33 Å). The clusters are subjected to the irradiation of a Gaussian-shaped laser pulse with a temporal half full width at a half maximum of 100 fs, similar to that in Ref. [23]. The initial phase of the field, Eq. (4), is taken as $\varphi_0=90°$.

The dynamics of cluster ionization and Coulomb explosion during the pulse irradiation is presented in Figs. 3 and 4 for the laser pulse intensity $10^{16}\,{\rm W/cm^2}$ and the frequency $\nu=0.386\,{\rm fs}^{-1}$. The inner ionization is characterized in these figures as the number of electrons per atom q_I removed from the atoms. The outer ionization is characterized as the number of electrons per atom q_O removed from the cluster to distance R_O Eq. (13). The Coulomb explosion is described as the time evolution of the mean-square root of the x coordinate of the cluster atoms, which is the coordinate of the laser field polarization,

$$X(t)=\sqrt{\frac{1}{n}\sum_{i=1}^{n} x_i^2}. \tag{15}$$

The x coordinate origin ($x=0$) lies at the cluster center of mass. The $X(t)$ value is presented in Fig. 4(c) as a dimensionless value, $X(t)/X(0)$.

The dynamics during the first 4 fs of the ionization process is presented in Fig. 3. The atoms begin to lose their electrons in the very beginning of the pulse so that during the first half circle of the laser radiation ($t\approx1.3$ fs) they are deprived, on average, of six to seven electrons; i.e., they are deprived from all six $5p$ electrons and sometimes also from one $5s$ electron. At $t=4$ fs, the inner ionization approaches the $q_I=8$ level, which implies that almost all of the outer shell $5s^25p^6$ electrons are already removed from their atoms. The inner ionization level at $t<1.5$ fs increases with the cluster size, but at $t>1.5$ fs it is nearly cluster size independent. The outer ionization begins with some delay, which is

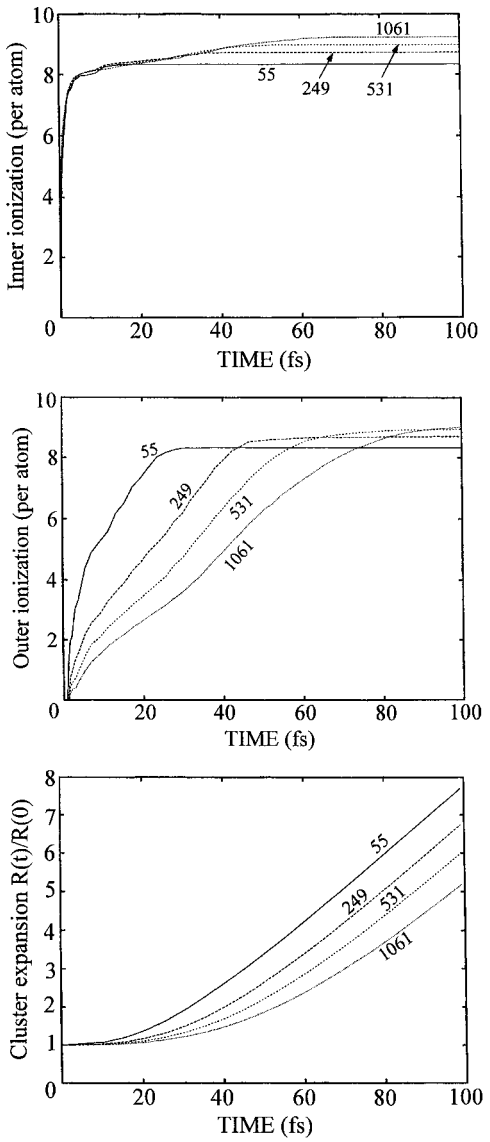

FIG. 4. Ionization dynamics during the whole pulse. The numbers indicate the cluster size. Irradiation parameters as in Fig. 1. (a) Inner ionization, (b) outer ionization, (c) cluster expansion.

$t_o = 0.93$, 1.08, 1.18, and 1.28 fs for Xe_{55}, Xe_{249}, Xe_{531}, and Xe_{1061}, respectively. The obvious reason for such a delay is the time the electrons need to overcome the R_O distance, Eq. (13), which increases with the cluster size. The t_o dependence on the number n of the cluster atoms is fitted satisfactorily by a simple equation:

$$t_o = \tau_o + Cn^{1/6}, \tag{16}$$

with $\tau_o = 0.366$ fs and $C = 0.286$ fs. Taking into account that R_O is proportional to $n^{1/3}$, we find that t_o depends linearly on $\sqrt{R_O}$. Such dependence indicates the uniformly accelerated electron motion in the time interval $\tau_o < t < t_o$. For all the clusters considered here, this time interval lies around the first maximum of the laser field [$\varphi = 180°$, Eq. (4)] where the field does not vary much, and it accelerates electrons outside the cluster in an almost uniform way.

TABLE I. The total number of electrons generated by the suppression and collisional mechanisms of the inner ionization. Irradiation parameters: maximal power, $S_{max} = 10^{16}$ W/cm^2; frequency, $\nu = 0.386$ fs^{-1}.

	Xe_{55}	Xe_{249}	Xe_{531}	Xe_{1061}
Suppression	458	2166	4745	9669
Collisional	0	5	20	117

The general picture of the ionization dynamics is displayed in Fig. 4. The inner ionization [Fig. 4(a)] crosses the level $q_I = 8$ at ~ 5 fs for all clusters. Further ionization is realized by the removal of the $4d$ electrons. Because of the large IP of these electrons, the process of the inner ionization is slowed down at $t > 5$ fs, reaching saturation at some longer time. The dependence of the saturation levels q_I on the cluster size is presented in Fig. 5. The saturation level q_I increases with the cluster size but not by much; namely, from $q_I = 8.33$ in Xe_{55} to $q_I = 9.22$ in Xe_{1061}. As we see only in the Xe_{1061} cluster, each atom loses on average more than one $4d$ electron. The total number of electrons released by the suppression and collisional mechanisms are presented in Table I. In contrast to the results of Ref. [23], we found that the contribution of the collisional ionization is of minor importance, making up for only 1.2% of the total ionization yield in the largest Xe_{1061} cluster, while in the Xe_{55} cluster we did not detect any event of collisional ionization.

The process of outer ionization proceeds much faster and the saturation level is reached much sooner in smaller clusters than in the larger ones [Fig. 4(b)]. Quantitatively, we define the saturation point t_s, presented in Fig. 5, somewhat arbitrarily, as the time when the ionization rate becomes smaller than ten electrons per femtosecond. The saturation point t_s is satisfactorily fitted by $(t_s)_{fit} = 2.95n^{1/2}$. The physical background for the $\sim n^{1/2}$ size dependence of t_s is not clear. Figure 5 also presents the outer ionization saturation level q_O's dependence on the cluster size. In the Xe_{55} cluster the saturation level of the outer ionization is the same as that of the inner ionization. In larger clusters the saturation level

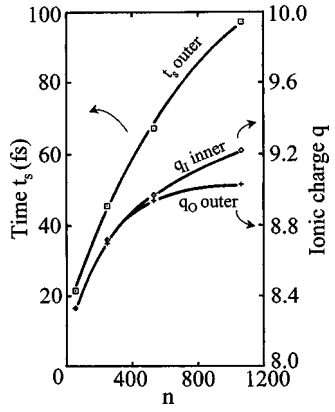

FIG. 5. Dependence of the inner and outer ionization saturation levels per atom (the right scale) and the saturation time t_s of the outer ionization process (the left scale) on the cluster size. Irradiation parameters as in Fig. 1.

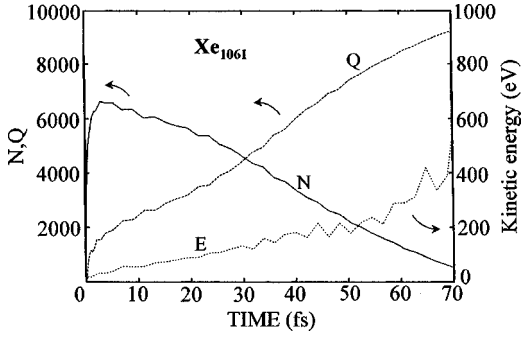

FIG. 6. Ionization dynamics inside the Xe_{1061} cluster. N is the total number of unbound electrons inside the cluster, Q is the cluster charge in the e-charge units (the left scale), and E is the average kinetic energy of electrons inside the cluster (the right scale). Irradiation parameters as in Fig. 1.

of the outer ionization is only a little lower than that of the inner ionization. This means that almost all electrons removed from their host atoms by the inner ionization are also removed from the cluster. This confirms the finding of our previous work [22]—that the inner ionization constitutes the bottleneck of the cluster ionization process.

Our calculations are based on the assumption that the outer laser field, Eq. (4), does not depend on coordinates. Such an assumption implies the neglect of the light absorption by the cluster. In order to check the validity of this assumption, we will estimate the light absorption in the largest of the clusters treated here, namely, Xe_{1061}. The gradient of the light intensity W inside the cluster is equal, with the opposite sign, to the rate of the energy losses per unit volume. Suggesting the energy losses E to be small and uniformly distributed inside the cluster, one obtains for the light intensity decrease along the propagation path Δx the expression

$$\Delta W = \frac{1}{V}\frac{dE}{dt}\Delta x, \tag{17}$$

where V is the cluster volume. At the very beginning of the pulse, the light absorption is caused almost solely by the inner ionization (Fig. 3) so that the decrease in the light intensity becomes

$$(\Delta W)_{\mathrm{ii}} = I^{(j)}\frac{1}{V(t)}\left(\frac{dN_{\mathrm{ii}}(t)}{dt}\right)\Delta x, \tag{18}$$

where $I^{(j)}$ is the IP of the dominant ion at the time moment t, and N_{ii} is the number of electrons released by the inner ionization process [see Eq. (14)]. Calculations using the data of Fig. 3 show that the light intensity decrease along the cluster radius ($\Delta x = 2R$) is $(\Delta W)_{\mathrm{ii}} \approx 6\times 10^{14}\,\mathrm{W/cm^2}$, which makes up for about 10% of the total light intensity W at $t = 0$. Such a small light intensity attenuation, which furthermore takes place during a very short time interval of 0.3–0.5 fs, can be neglected. At $t > 1.5$ fs, the light absorption is mainly caused by the outer ionization process. In this case the light intensity decrease becomes

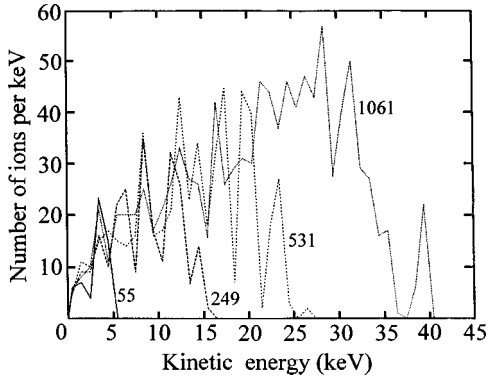

FIG. 7. Kinetic energy distribution of product ions. Irradiation parameters as in Fig. 1.

$$(\Delta W)_{\mathrm{oi}} = E_{\mathrm{oi}}(t)\frac{1}{V(t)}\left(\frac{dN_{\mathrm{oi}}(t)}{dt}\right)\Delta x, \tag{19}$$

where N_{oi} is the number of electrons removed from the cluster by the outer ionization process and E_{oi} is the energy of an electron removal from the cluster surface to infinity:

$$E_{\mathrm{oi}}(t) = B\frac{Q(t)}{R(t)}, \tag{20}$$

where $Q(t)$ is the total cluster charge and $R(t)$ is the cluster radius. Using the data of Figs. 4(b), 4(c), and 6 we found that $(\Delta W)_{\mathrm{oi}}$ reaches its maximum at $t \sim 35$ fs where it is $(\Delta W)_{\mathrm{oi}} \approx 2.4\times 10^{14}\,\mathrm{W/cm^2}$ or only about 3% of the total light intensity $W(t)$ at $t = 35$ fs. At $t > 45$ fs the light absorption begins to decrease strongly due to the increase in the cluster volume $V(t)$ [Fig. 4(c)]. The electron gas heating (Fig. 6) also contributes to the light absorption but to a very small extent, according to our estimates. The analysis we performed supports our assumptions, which neglect the light attenuation inside the cluster.

The dynamics of the cluster expansion is shown in Fig. 4(c). The cause of the cluster expansion is the Coulomb repulsion between ions in a charged cluster. The charge of the clusters increases in the process of the outer ionization. Thus the charge of the Xe_{1061} cluster jumps almost immediately, at the time scale of ~ 3 fs, to the level of about $Q = 1000$ (in e-charge units), but after this jump it begins to increase relatively slowly until it reaches the saturation level (Fig. 6). The increase of the cluster charge strengthens the Coulomb repulsion forces between ions and consequently the acceleration of the cluster expansion. As a result, the cluster size increases as $[R(t)/R(0)-1] \sim t^3$, whereas in the case of a constant charge it increases as $[R(t)/R(0)-1] \sim t^2$ [14]. The expansion, however, increases the interionic distances and contributes to the weakening of the Coulomb repulsion forces. At some instant this effect compensates for the effect of the charge increase so that the acceleration begins to decrease and finally the expansion becomes uniform. In the small Xe_{55} cluster, the expansion is already uniform after the middle of the pulse, whereas in the Xe_{1061} cluster it happens only at the pulse's end [Fig. 4(c)]. We suggest describing the

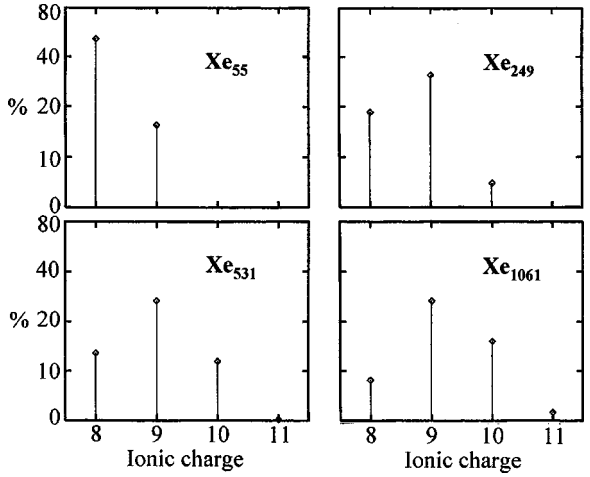

FIG. 8. Charge distribution of product ions. Irradiation parameters as in Fig. 1.

expansion dependence on t, which fits both the small and large t behavior, using the expression

$$\frac{R(t)}{R(0)} = 1 + \frac{\alpha t^3}{1+\beta t+\gamma t^2}. \tag{21}$$

In the Xe_{1061} case, the parameters of Eq. (21) were found to be $\alpha = 10^{-5}\ \mathrm{fs}^{-3}$, $\beta = 3.11\times10^{-3}\ \mathrm{fs}^{-1}$, $\gamma = 1.02\times10^{-4}\ \mathrm{fs}^{-2}$.

Figure 4(c) presents the expansion along the x axis, the axis of the light polarization. The expansion along the two other axes is a little smaller than that along the x axis. Using the cluster radii R_x and R_y (the radii R_y and R_z were found to be equal) we define the anisotropy parameter as

$$\chi = (R_x - R_y)/R_x. \tag{22}$$

The anisotropy parameters at the end of the pulse were found to be equal to $\chi = 0.065$, 0.080, 0.084, and 0.084 for Xe_{55}, Xe_{249}, Xe_{531}, and Xe_{1061}, respectively.

The final kinetic-energy distributions of ions are shown in Fig. 7. The distributions demonstrate pronounced oscillations, which are associated with the cluster shells or subshells. Thus in the case of the Xe_{55} cluster, the small peak is connected with the 12 atoms of the second atomic shell and the large peak is connected with the 42 atoms of the third atomic shell. The maximal kinetic energy of the product ions increases with the cluster size. Thus it is only 5 keV in the case of the Xe_{55} cluster but about 40 keV in the case of the Xe_{1061} cluster.

The distribution of the final (saturation level) ionic charges is shown in Fig. 8. The minimal charge in all clusters is $q_I = 8$, which means that all atoms lose their $5s$ and $5p$ electrons. In the Xe_{55} cluster, only two kinds of product ions appear, namely, Xe^{8+} ($\sim$70%) and Xe^{9+} ($\sim$30%), the last one due to the loss of one $4d$ electron. In the Xe_{249} cluster a small number of Xe^{10+} ions appear and the distribution maximum is shifted to $q_I = 9$, while in the Xe_{531} and Xe_{1061} clusters the maximum lies at $q_I = 9$ but the maximal ionic charge reaches $q_I = 11$, reflecting the increased contribution of the ionization of $4d$ electrons.

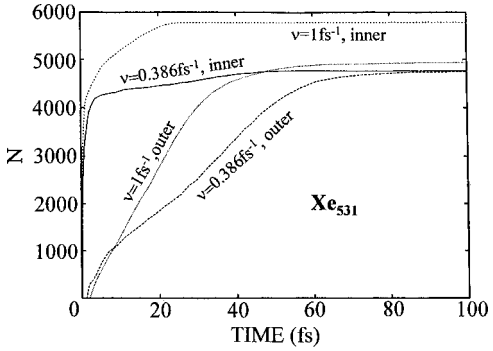

FIG. 9. Ionization dynamics of the Xe_{531} cluster for two laser frequencies: $\nu = 0.386$ and $\nu = 1.0\ \mathrm{fs}^{-1}$ and the power $S_{\max} = 10^{16}\ \mathrm{W/cm^2}$. The inner and outer ionization processes are presented as the total number of electrons removed from the host atoms and the cluster, respectively.

In order to study the effect of light frequency on the ionization, we performed a simulation for the Xe_{531} cluster at the frequency $\nu = 1.0\ \mathrm{fs}^{-1}$. The ionization dynamics at two frequencies, $\nu = 0.386$ and $\nu = 1.0\ \mathrm{fs}^{-1}$, are compared in Fig. 9. In the beginning of irradiation, the ionization efficiency is much higher at $\nu = 1.0\ \mathrm{fs}^{-1}$ than at $\nu = 0.386\ \mathrm{fs}^{-1}$. The increase in the ionization efficiency results in the production of ions with higher charge and energy. Thus the maximal values of ionic charge and energy at $\nu = 1.0\ \mathrm{fs}^{-1}$ are $q_I = 13$ and $E_k \approx 40$ keV, respectively, compared with $q_I = 11$ and $E_k \approx 27$ keV for the lower $\nu = 0.386\ \mathrm{fs}^{-1}$ frequency.

The dependence of the ionization efficiency on the light power has been studied for the Xe_{249} cluster. The results of this study are shown in Table II. Even at a power as low as $S_{\max} = 10^{14}\ \mathrm{W/cm^2}$, all atoms are deprived of all of their outer shell electrons. The level of the outer ionization is, however, low at this power, making up for only 11.2% of the total number of electrons released by the inner ionization. As a result of the relatively high level of inner ionization and the low level of outer ionization, the electrons form a dense and almost neutral plasma inside the cluster. The increase of the power to $S_{\max} = 10^{15}\ \mathrm{W/cm^2}$ and even to $S_{\max} = 10^{16}\ \mathrm{W/cm^2}$ does not raise by much the inner ionization level but increases significantly the outer ionization efficiency, so that practically all electrons generated by the inner ionization are removed from the cluster. Only the increase of the power to $S_{\max} = 10^{17}\ \mathrm{W/cm^2}$ significantly affects the inner ionization,

TABLE II. Multielectron ionization of Xe_{249}. Final numbers of the inner (N_1) and outer (N_O) ionizations, the average (q_{av}) and maximal ($q_{\max}$) charges of the product ions, and the kinetic energy of these ions for different laser irradiation powers $S_{\max}$. The laser frequency is $\nu = 0.386\ \mathrm{fs}^{-1}$.

$S_{\max}$ ($\mathrm{W/cm^2}$)	$eF_{\max}$ (eV/Å)	N_I	N_O	q_{av}	$q_{\max}$	$E_{\max}$ (keV)
10^{14}	2.74	1992	227	8.00	8	3
10^{15}	8.68	1994	1994	8.01	9	9
10^{16}	27.4	2171	2167	8.72	10	16
10^{17}	86.8	3364	3364	13.5	17	40

providing ions as highly charged as $q_I=17$. The maximal kinetic energy of ions is also high, about 40 keV, like in the Xe_{1061} cluster at $S_{max}=10^{16}$ W/cm^2.

IV. DISCUSSION

Three processes—inner ionization, outer ionization, and Coulomb explosion—determine the dynamics of the cluster ionization. All these processes are usually strongly coupled, which complicates the interpretation of the mechanisms involved. We will try, however, to describe the results of our simulation in terms of physical phenomena that affect the cluster ionization and decay.

The first stage of the cluster ionization is the inner ionization by the suppression mechanism (Fig. 3). Initially, the bound electrons are removed from their host atoms by the direct effect of the laser field, whose amplitude is about 20 eV/Å at the beginning of the simulation for $S_{max}=10^{16}$ W/cm^2. Such a field, according to Eq. (5), can remove from a Xe atom all six $5p$ electrons (IP$\leqslant$71.87 eV) but none of the $5s$ electrons (IP=92.1 and 105.9 eV). The results presented in Fig. 3 show that the inner ionization level really becomes close to $q_I=6$ at $t=0.65$ fs when the laser field reaches its first amplitude value. The unbound electrons generated by the inner ionization form no equilibrium plasma with a nonuniform charge distribution, which generates an inner field. This field, according to the ignition mechanism, enhances the inner ionization. The $5s$ electrons, as well as the stronger bound $4d$ electrons (IP$\geqslant$171 eV), can be removed only by the combined effect of the outer (laser) field and the inner field. Due to this effect, the average ionic charge q_I continues to increase, crossing in all clusters the level of $q_I\approx 8$ at $t\sim 5$ fs [Fig. 4(a)]. A further increase in the average ionic charge develops very slowly since it is connected with the removal of the strongly bound $4d$ electrons.

In the very beginning of the ionization process the cluster is neutral so that some of the unbound electrons may easily leave the cluster, which then becomes positively charged. While the cluster charge is still small, the inner fields are determined mainly by the charge fluctuations. These fluctuations are expected to be stronger in large clusters, contributing to a higher level of the inner ionization in these clusters (Fig. 3). A further increase in the cluster charge results in two effects. First, the electron attraction to the cluster becomes stronger, which slows down the increase of the cluster charge (Fig. 6) and the rate of the outer ionization (Fig. 3). Second, the inner fields become stronger, contributing to the increase of the inner ionization level. In small clusters the process of outer ionization goes faster (Fig. 3), leading to a faster increase of their charge and, consequently, of the inner fields. As a result, the inner ionization level in small clusters rises quickly to the level of large clusters and in the interval $t\approx 1.5-20$ fs the inner ionization levels in all clusters become almost the same [Fig. 4(a)].

The increase of the cluster charge not only enhances the inner ionization but also accelerates the cluster expansion, resulting in the increase of interionic distances and the weakening of the ignition mechanism effect. In the smallest cluster Xe_{55}, the total charge is relatively small; for example, $Q_c=440$ when the average ionic charge is $q_I=8$ and all unbound electrons are outside the cluster. The inner field generated by this charge cannot contribute to the removal of a significant number of $4d$ electrons even in the neutral cluster geometry. Consequently, the inner ionization process stops quickly, already at $t\sim 12$ fs [Fig. 4(a)]. Around the same time the cluster size begins to increase, but it is already not of any importance for the inner ionization process. The situation is different in larger clusters, which can bear larger charge Q_c.

Let us now consider the largest cluster Xe_{1061}. At $t=10$ fs, the charge of this cluster is about $Q_c\sim 2500$ (Fig. 6). Such a charge generates the inner fields of about 40–50 eV/Å, which can contribute noticeably to the removal of $4d$ electrons. At $t>10$ fs, the cluster charge continues to rise leading to a further increase in the inner ionization level [Fig. 4(a)]. However, at $t>40$ fs the cluster size begins to increase quickly, being doubled at $t\approx 58$ fs [Fig. 4(c)]. The increase in the cluster size significantly weakens the inner fields. Consequently, the inner ionization process almost stops around $t\sim 60$ fs [Fig. 4(a)]. In the Xe_{249} and Xe_{531} clusters the inner ionization process also stops due to the expansion of these clusters; however, this happens sooner than in the Xe_{1061} cluster, since in these clusters the expansion goes faster than in the Xe_{1061} cluster [Fig. 4(c)].

As mentioned before, the increase of the cluster charge due to the process of the outer ionization strengthens the electrons bound to the cluster. Consequently, the rate of the outer ionization decreases at the time scale of 1–2 fs (Fig. 3). The increase of the cluster charge also continues at $t>2$ fs and one would think that this would hamper the subsequent ionization process. However, this is not the case as quite the opposite takes place, at least in the Xe_{1061} cluster, where even the outer ionization rate increases, although slightly, in the interval of $\sim$30–40 fs [Fig. 4(b)]. The reason for such strange behavior of the outer ionization lies in the quasiresonance mechanism of this phenomenon [21,22]. The simulation of the outer ionization process previously performed by us showed that in the Xe_{1061} cluster the quasiresonance mechanism leads to a strong increase in the ionization efficiency when the cluster radius increases to $R\sim(1.4-1.8)R_0$ [22]. The interval of the outer ionization rate increase found in the present simulation ($t\sim 30-40$ fs) corresponds to a somewhat smaller cluster radii, $R\sim(1.3-1.6)R_0$ [Fig. 4(c)]. In the Xe_{249} and Xe_{531} clusters the outer ionization rate in the wide interval of 5–45 fs is almost constant, probably due to the mutual compensation of different factors. In the case of the Xe_{55} cluster, there is no indication whatsoever of the quasiresonance process.

The character of the electron motion, which leads to the outer ionization, is well demonstrated by three trajectories of the Xe_{531} cluster electrons (Fig. 1). Trajectory (a) demonstrates an early electron removal from the cluster at $t\approx 3$ fs, when the cluster charge is very small and electrons are weakly bound to the cluster. In this case the outer field can easily remove an electron from the cluster, demonstrating the one-way ionization process [21]. Trajectory (b) demonstrates an electron, which is removed from the cluster in the middle of the outer ionization process [Fig. 4(b)], at $t\sim 38$ fs. At this

time the cluster expansion is noticeably promoted and the cluster size is roughly 50% larger than the initial one [Fig. 4(c)]. Up to the time of $t \sim 36$ fs the electron moves inside the cluster, going out from the cluster only occasionally and to a very small distance from its surface. The electron motion is strongly affected by collisions, which prevent an enhancement of the electron energy. In some intervals the electron gets enough energy to avoid collisions and demonstrate almost regular oscillations. These oscillations, however, are not in a phase with the laser field. Only at $t \sim 33.5$ fs, probably due to the larger cluster size, does the electron begin to oscillate in a phase with the laser field, contributing to the increase of the electron oscillation amplitude (in the three subsequent oscillations it is 10, 36, and 360 Å). At the same time energy is enhanced (the three subsequent energy peaks are 320, 350, and 780 eV, Fig. 2). During these oscillations the electron crosses the cluster four times, but due to the high energy it avoids collisions that could perturb the process of the energy enhancement. Such a process of energy enhancement, which leads finally to the ionization, is of a clear quasiresonance character. The ionization process is different in trajectory (c), where the electron is removed from the cluster by one swing at $t \sim 52$ fs. At this time the cluster expansion is very advanced and the cluster size is about 2.5 times larger than in the neutral cluster [Fig. 4(c)]. The strong increase of the cluster volume (about 15 times) significantly reduces the probability of collisions, which facilitates the energy enhancement.

The trajectories demonstrate a strong effect of collisions on the electron energy enhancement process. The collision effect decreases strongly with the increase of kinetic energy E_k, and at roughly $E_k > 100$ eV an electron is expected to move almost freely inside the cluster [21]. The kinetic energy of trajectory (b), for example, is mostly lower than 100 eV (Fig. 2) so that the electron is subjected to numerous collisions until its energy becomes high at $t \sim 35$ fs. It is possible to conclude that the effect of the cluster expansion on the electron energy enhancement is double. The increase of the cluster size (due to the Coulomb explosion) decreases the frequency of the electron oscillations inside the cluster, promoting the conditions of the quasiresonance energy enhancement [21,22]. At the same time, because of the cluster density decrease, the probability of collisions becomes less, reducing the hampering effect of the collisions on the energy enhancement and also promoting the outer ionization process.

ACKNOWLEDGMENT

This research was supported by the Binational German-Israeli James Frank Program on Laser-Matter Interaction.

[1] *The Physics and Chemistry of Small Clusters*, edited by P. Jena, B. K. Rao, and S. N. Khanna (Plenum, New York, 1986).
[2] *Physics and Chemistry of Finite Systems: From Clusters to Crystals*, edited by P. Jena, S. N. Khanna, and B. K. Rao (Kluwer, Dordrecht, 1992).
[3] *Large Finite Systems*, edited by J. Jortner, A. Pullman, and B. Pullman (Reidel, Dordrecht, 1987).
[4] K. Codling, L. J. Frasinski, P. Hatherly, and J. R. M. Barr, J. Phys. B **20**, L525 (1987).
[5] K. Boyer, T. S. Luk, J. C. Solem, and C. K. Rhodes, Phys. Rev. A **39**, 1186 (1989).
[6] D. Normand and M. Schmidt, Phys. Rev. A **53**, R1958 (1996).
[7] J. Purnell, E. M. Snyder, S. Wei, and A. W. Castleman, Jr., Chem. Phys. Lett. **229**, 333 (1994).
[8] J. Kou, N. Nakashima, S. Sakabe, S. Kawato, H. Ueyama, T. Urano, T. Kuge, Y. Izawa, and Y. Kato, Chem. Phys. Lett. **289**, 334 (1998).
[9] T. Ditmire, J. W. G. Tisch, E. Springate, M. B. Mason, N. Hay, R. A. Smith, J. Marangos, and M. H. R. Hutchinson, Nature (London) **386**, 54 (1997).
[10] T. Ditmire, J. W. G. Tisch, E. Springate, M. B. Mason, N. Hay, J. P. Marangos, and M. H. R. Hutchinson, Phys. Rev. Lett. **78**, 2732 (1997).
[11] M. H. R. Hutchinson, T. Ditmire, E. Springate, J. W. G. Tisch, Y. L. Shao, M. B. Mason, N. Hay, and J. P. Marangos, Philos. Trans. R. Soc. London, Ser. A **356**, 297 (1998).
[12] T. Ditmire, E. Springate, J. W. G. Tisch, Y. L. Shao, M. B. Mason, N. Hay, J. P. Marangos, and M. H. R. Hutchinson, Phys. Rev. A **57**, 369 (1998).
[13] M. Lezius, S. Dobosh, D. Normand, and M. Schmidt, Phys. Rev. Lett. **80**, 261 (1998).
[14] I. Last, I. Schek, and J. Jortner, J. Chem. Phys. **107**, 6685 (1997).
[15] T. Ditmire, T. Donnelly, A. M. Rubenchik, R. W. Falcone, and M. D. Perry, Phys. Rev. A **53**, 3379 (1996).
[16] T. Zuo, S. Chelkowski, and A. D. Bandrauk, Phys. Rev. A **48**, 3837 (1993).
[17] T. Zuo and A. D. Bandrauk, Phys. Rev. A **52**, R2511 (1995).
[18] I. Last and J. Jortner, Phys. Rev. A **58**, 3826 (1998).
[19] S. Chelkowski and A. D. Bandrauk, J. Phys. B **28**, L723 (1995).
[20] T. Seideman, M. Yu. Ivanov, and P. B. Corkum, Phys. Rev. Lett. **75**, 2819 (1995).
[21] I. Last and J. Jortner, J. Phys. Chem. **102**, 9655 (1998).
[22] I. Last and J. Jortner, Phys. Rev. A **60**, 2215 (1999).
[23] T. Ditmire, Phys. Rev. A **57**, R4094 (1998).
[24] L. V. Keldysh, Zh. Eksp. Teor. Fiz. **47**, 1945 (1964) [Sov. Phys. JETP **20**, 1307 (1965)].
[25] P. E. Siska, J. Chem. Phys. **71**, 3942 (1979).
[26] A. Goldberg, I. Last, and T. F. George, J. Chem. Phys. **100**, 8277 (1994).
[27] C. Rose-Petruck, K. J. Schafer, K. R. Wilson, and C. P. J. Barty, Phys. Rev. A **55**, 1182 (1997).
[28] W. Lotz, Z. Phys. **216**, 241 (1968).